Wireline log signatures of resedimented volcaniclastic facies, ODP Leg 129, West Central Pacific

A. R. M. SALIMULLAH & D. A. V. STOW
Geology Department, The University, Southampton SO9 5NH, UK

Abstract. During Ocean Drilling Program Leg 129, two sites (800, 801) were drilled in Pigafetta Basin and one site (802) in East Mariana Basin, West Central Pacific. At all three sites, a thick (192–211 m) Cretaceous succession of dominantly volcaniclastic sediments was encountered, and at site 802 a further 222 m of Miocene–Pliocene volcaniclastics were drilled. These sediments are composed mainly of volcaniclastic material that has been resedimented downslope by various mass-flow processes including slumps, debris flows and turbidity currents. Sedimentary structures and textural variations observed in the recovered section can be used to calibrate the corresponding high-resolution Formation Micro-Scanner (FMS*) images and Dipmeter Micro-resistivity readings. Gamma ray log shapes show grain size evolution within a facies. Fining-upwards and coarsening-upwards grain size trends are observed for some sequences of turbidites and debrites. No obvious change in grain size is observed through massive structureless sandstones. CCA (calcium yield in decimal fraction) and CSI (silicon yield in decimal fraction) readings from the geochemical combination logs, correlated with visual compositional data, are useful to define calcareous and siliceous turbidite facies. This combination of wireline logs has been used in the poorly recovered intervals of volcaniclastic section in the ODP Leg 129 sites to improve significantly our understanding of basinal sedimentation and tectonics in the area.

During Leg 129 of the Ocean Drilling Program (ODP), three sites were drilled in the West Central Pacific. Sites 800 and 801 were drilled in Pigafetta Basin, and site 802 in East Mariana Basin, at present day water depths ranging from 5673.8 to 5968.6 m (Fig. 1). The average core recovery was poor, ranging from 17 to 29%. The lithostratigraphy of these sites, as summarized by the shipboard scientists (Lancelot, Larson *et al.* 1990) is shown in Fig. 2. A thick (192–211 m) succession of Cretaceous mainly volcaniclastic sediments was encountered in all three sites, together with a Miocene–Pliocene (222 m) volcaniclastic succession at site 802. These sediments can be divided into seven process-related facies on the basis of texture, structure and composition delineated from recovered portions of cores and/or with information provided by wireline log measurements. The facies are: debrites, slumps, massive sandstones with fluid escape structures, massive structureless sandstones, volcaniclastic turbidites, calcareous volcaniclastic turbidites, and bioclastic (radiolarian) turbidites and pelagites. These facies are typical of deep-water slope and basinal environments (e.g. Stow 1985, 1986), the volcaniclastic and bioclastic composition being common to mid-ocean or active margin settings (e.g. Kelts & Arther 1981).

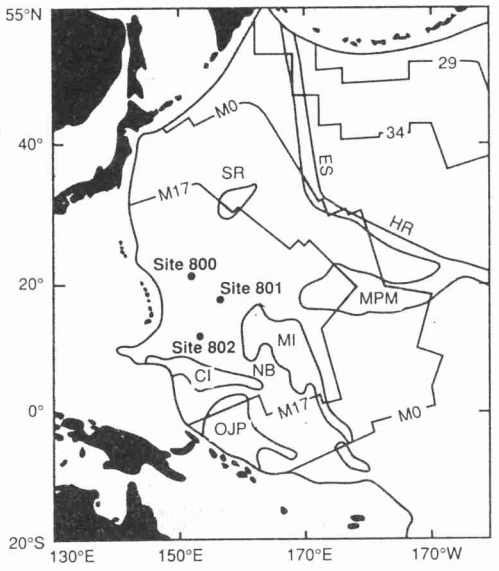

Fig. 1. Location map of Leg 129 Sites 800, 801, and 802. Bedrock isochrons are determined from the magnetic anomaly lineation mapping on the Pacific plate (after Larson *et al.* 1985) and superimposed on groups of islands, attols and guyots in the western Pacific Ocean. (Feature abbreviations are as follows: Caroline Islands (CI), Ontong Java Plateau (OJP), Marshall Islands (MI), Nauru Basin (NB), Mid-Pacific Mountains (MPM), Shatsky Rise (SR), Hawaiian Ridge (HR) and Emperor Seamounts (ES).

* Mark of Schlumberger

From HURST, A., GRIFFITHS, C. M. & WORTHINGTON, P. F. (eds), 1992, *Geological Applications of Wireline Logs II.* Geological Society Special Publication No. 65, pp. 87–97.

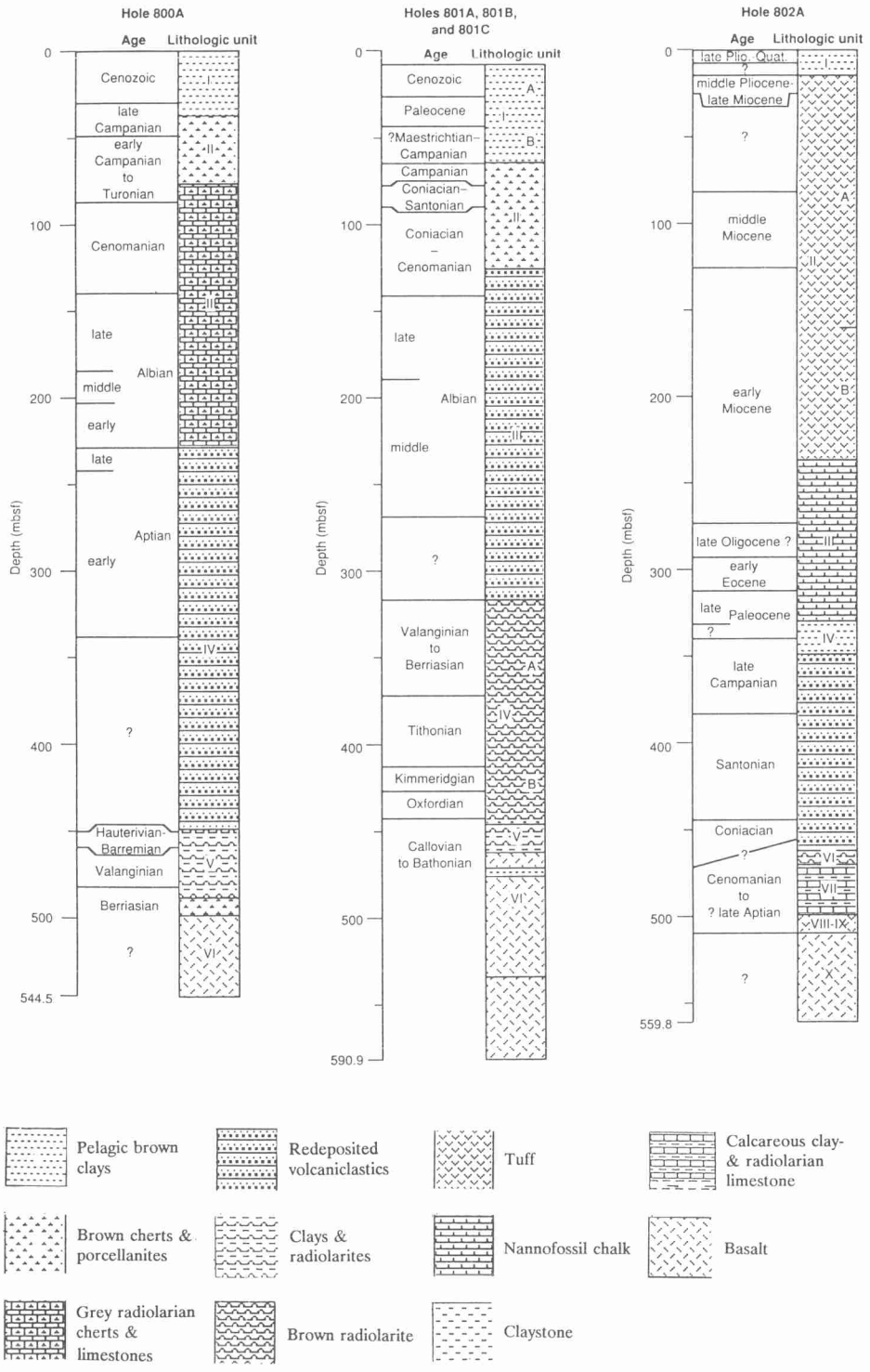

Fig. 2. Summary lithostratigraphy of ODP sites 800, 801 and 802.

Following the normal ODP continuous coring operation, an extensive suite of wireline logs was run at each site in open hole conditions, using small diameter (3.625 in^3/9.2 cm^3) borehole tools (Lancelot, Larson *et al.* 1990). The following data set was therefore available for use in this study:

Core and laboratory data

(A) visual core descriptions (V C D)
(B) core photos
(C) thin section data

Wireline log data

(D) Formation MicroScanner (FMS) images (scale: 1/5)
(E) Dipmeter Micro-resistivity logs
(F) Gamma ray logs
(G) Geochemical logging tool
  (i) CSI (silicon yield in decimal fraction)
  (ii) CCI (calcium yield in decimal fraction)
  (iii) LIR (lithology indicator ratio–silica/silica + calcium).

The FMS, Dipmeter-Microresistivity and gamma ray logs are used in this study to provide information on the texture and structure of the sediments, whereas the geochemical logs are used to give information on their composition. It must be recognized that the generally very high porosities of volcaniclastic sediments serve to degrade the geochemical signatures. There have been very few published studies of wireline log traces through volcaniclastic successions (e.g. Stow 1984).

The primary objectives of this study, are therefore: (a) to document the signatures of various wireline logs in the different facies present within the volcaniclastic units, having first compared these carefully with the recovered cores; (b) to show how various combinations of logs can be used to enhance the delineation of facies within the volcaniclastic sediments.

Core–log correlation metholodogy

The FMS tool provides the high resolution and continuous downhole borehole coverage necessary to distinguish fine bedding, internal bed structures and subtle changes in rock properties (Ekstrom *et al.* 1986). However, it is still crucial to integrate core data with open hole logs (Harker *et al.* 1990) to confidently establish lithological changes related to log trends. The general core–log correlation and interpretation approach adopted was as follows.

(a) Common sedimentary features, such as graded bedding, lamination, bioturbation etc. within the various facies observed in recovered cores were correlated with the FMS images. These images were also compared with previously published FMS interpretations (e.g. Serra 1986, 1989; Luthi 1990). In this way we were able to build up a database, for this suite of sediments, of FMS images and corresponding sedimentary interpretations.

(b) In the intervals where there was no recovery of cores, the FMS images were compared with the database developed in (a), hence allowing an interpretation of the non-recovered section.

(c) Dipmeter arrow plots (angle and azimuth) were examined for each facies, especially noting the vertical evolution and distribution of dips. Different facies show different dipmeter patterns, so it is possible to distinguish between facies. Distinctive trends may also be related to changes in rock properties (e.g. grain size) within and between individual beds.

(d) Microresistivity log readings were examined, especially to identify homogeneity and heterogeneity in terms of grain size for the massive structureless sediments recognized from core and images.

(e) Gamma ray log responses were correlated with the various facies, noting especially any vertical trends in terms of grain size.

(f) Higher CCA (calcium yield in decimal fraction) log readings were correlated with the core and thin section data in order to locate carbonate-rich intervals and to help identify possible calcareous volcaniclastic turbidites.

(g) Higher CSI (silica yield in decimal fraction) log readings were correlated with the core and thin section data with a view to locating siliceous intervals (e.g. clayey radiolarites/radiolarian claystones) and to help distinguish pelagites from pelagic/bioclastic turbidites in terms of composition.

(h) LIR (lithology indicator ratio) log readings were used to show the bulk compositional evolution of certain facies and to help establish the composition of the background sediments, in order to provide information on biological (production) and chemical (CCD/SCD) aspects of the oceanic environments during volcaniclastic sedimentation.

Sediment facies and wireline log signatures

Debrites

This facies occurs in relatively thick (70–150 cm), structureless beds that are poorly sorted

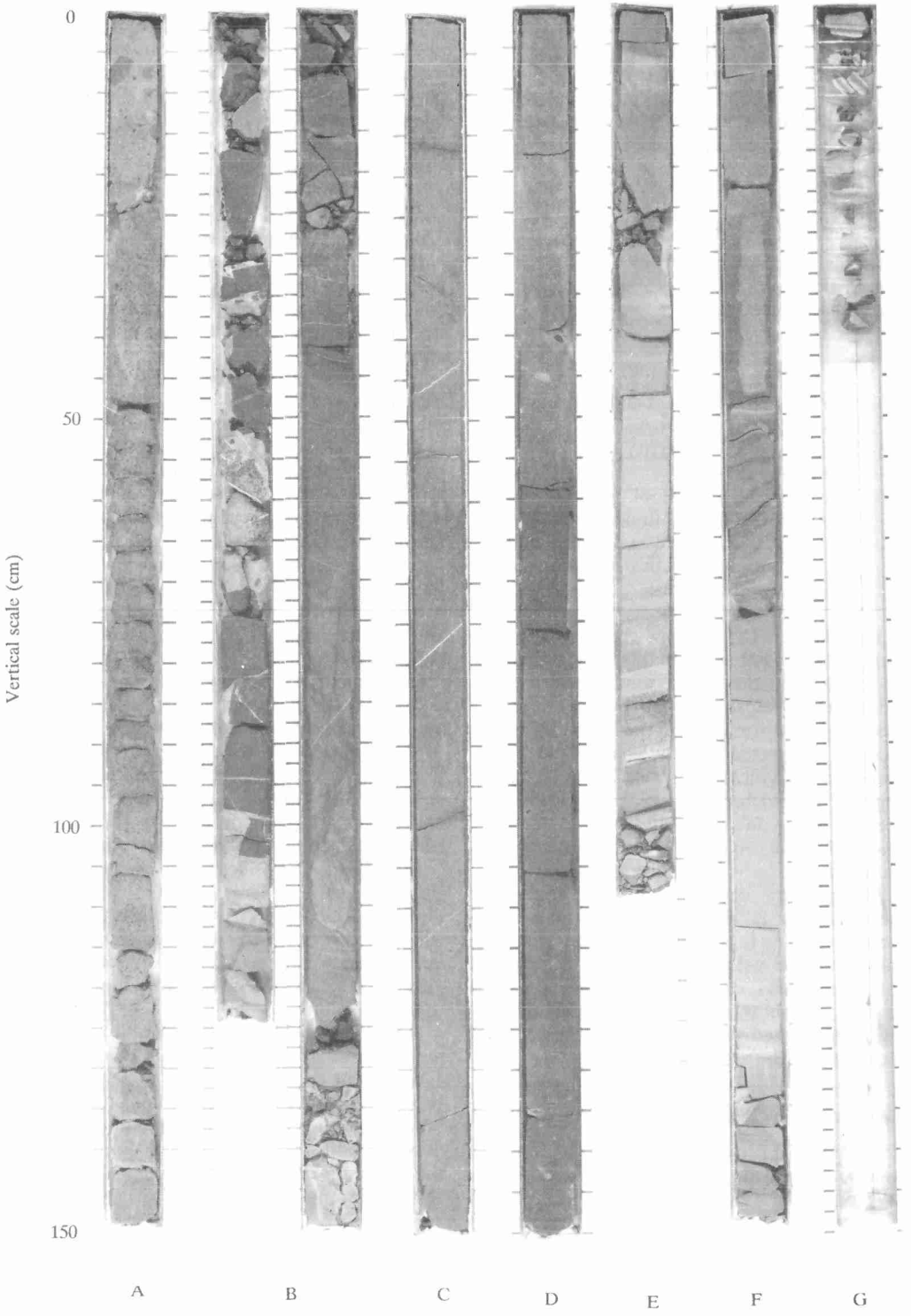

Fig. 3. Core photographs of volcaniclastic facies: A, debrites; B, slumps; C, massive sandstones with fluid escape structures; D, massive structureless sandstones; E, volcaniclastic turbidites; F, calcareous volcaniclastic turbidites; G, pelagites.

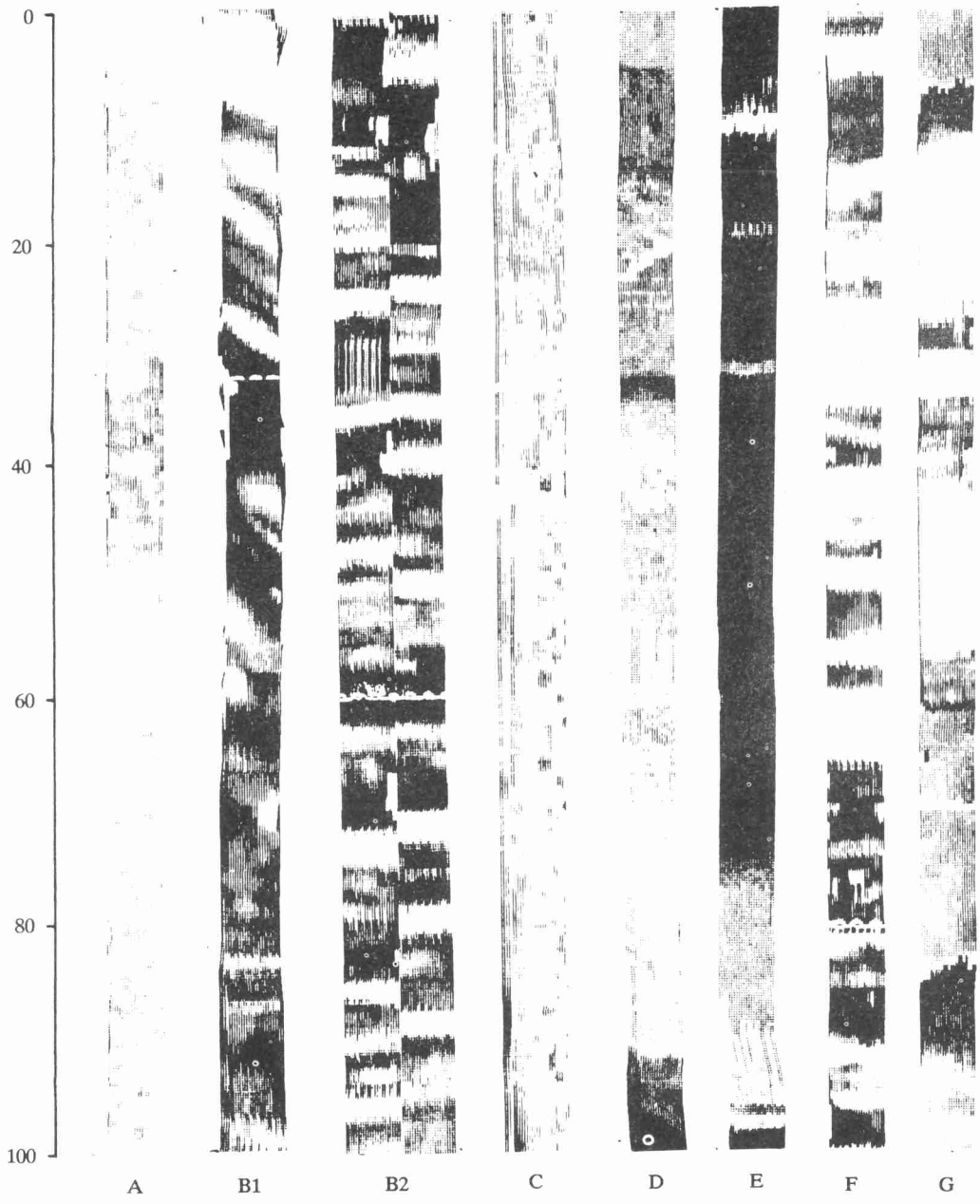

Fig. 4. Characteristic FMS images of volcaniclastic facies: A, debrites, B, slumps; B1 microfolds (recumbent); B2, microfaults; C, massive structureless sandstones; D, volcaniclastic turbidites; E, calcareous volcaniclastic turbidites; F, pelagites; G, bioclastic turbidites.

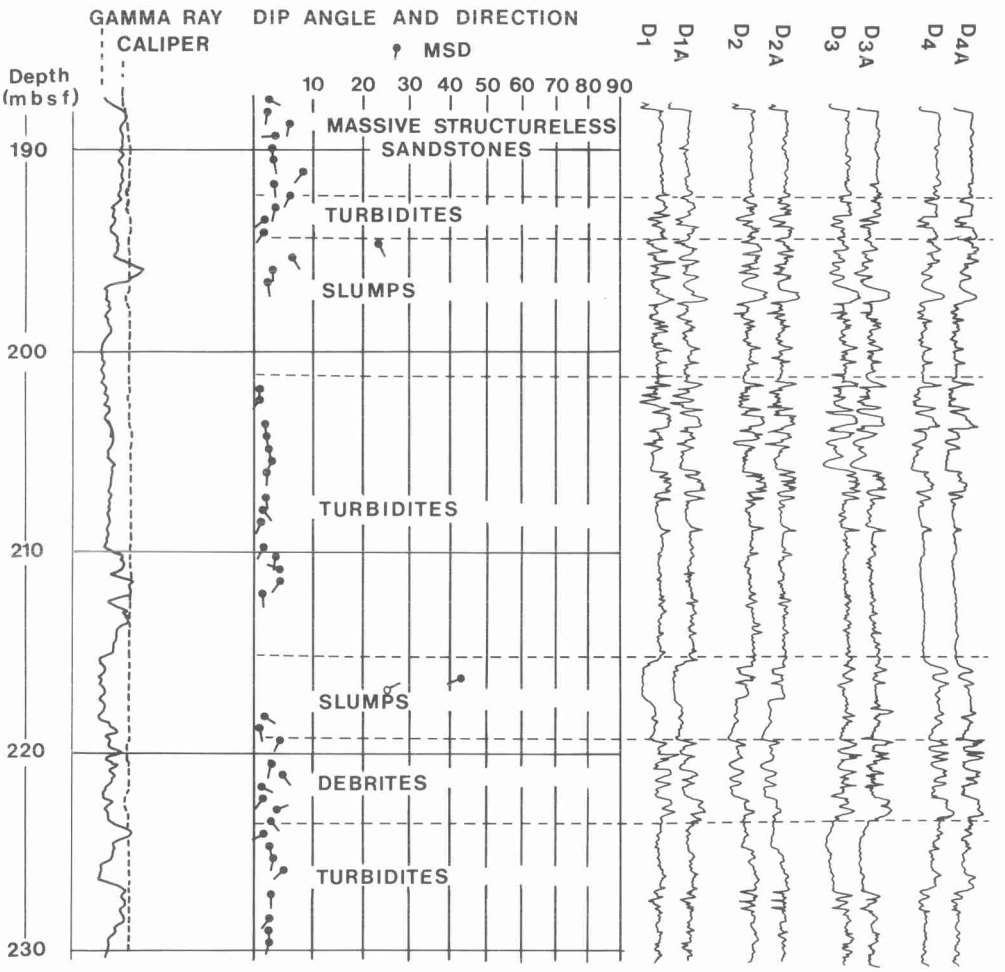

Fig. 5. Dipmeter plots and micro-resistivity log readings of volcaniclastic facies from ODP Hole 801B.

with random fabrics and poor grading (Fig. 3A). The matrix is clay to sand size and is composed of smectite/chlorite clays and volcanic glasses. The clasts are very coarse sand to pebble size, sub-rounded to well rounded and are mainly composed of muds (mud clasts) and igneous rock fragments.

FMS images show an uneven distribution of white (more resistive) irregular patches or dots (clasts/pebbles) in a dark/black (more conductive) medium or matrix, and confirm the heterogeneous and structureless natures of the beds. The shape of these white patches (dots, subrounded to rounded or angular) helps distinguish between conglomerate and breccia and also helps to distinguish conglomerate/breccia from bioturbational mottles which can create a similar FMS image. Figure 4A shows that the white patches (dots) are subrounded to rounded in shape which indicates the presence of conglomerates. Where there is a relatively higher abundance of closely spaced white patches (dots), this indicates clast-supported conglomerates, whereas a lower abundance is indicative of matrix-supported conglomerates.

For the very thick-bedded debrites, these features can also be seen on other logs. Dipmeter plots reveal variable dips and azimuths throughout the debrite intervals (Fig. 5). Micro-resistivity curves show the heterogeneous nature of debrite beds with an absence of correlation between the different traces in some instances

(Serra 1985). Where clasts/mudclasts are close to each other (clast-supported conglomerates), the peaks are relatively close (Fig. 4A); but where the clasts are isolated in a sandy or silty/clayey matrix, the peaks are isolated and/or absent. Gamma ray logs (Fig. 6) show both serrated and relatively smooth parts of different debrite beds, again indicating variable grain/clast size and both clast-supported and matrix-supported conglomerates, respectively. The responses also reveal general coarsening-upward sequences of debrites in some intervals of Hole 801B. LIR (lithology indicator ratio) log readings reveal distinct fluctuations in silica content within these sequences.

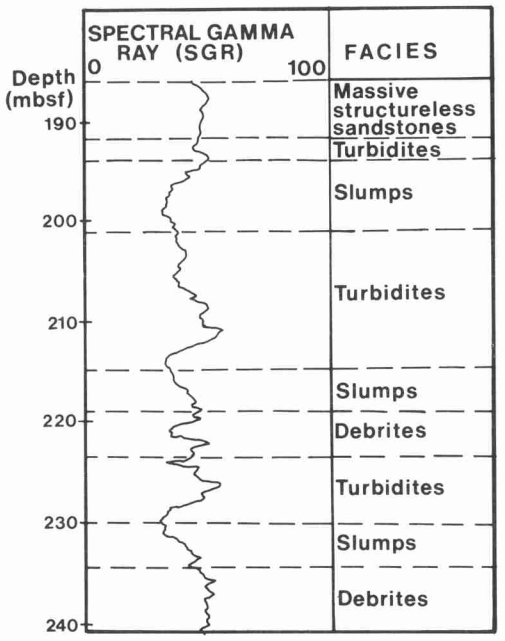

Fig. 6. Gamma ray log readings of volcaniclastic facies from ODP Hole 801B.

Slumps

There was very little recovery of the sediments in those intervals which are thought to be related to sliding or slumping on the basis of their wireline log responses. Two possible intervals from which cores had been recovered are shown in Fig. 3B. However, the FMS images reveal unique features of slumps including microfolds (Luthi 1990) and microfaults. The geometry and shape of the images provide evidence of recumbent slump folds (Fig. 4B1), accompanied by probable water escape features, steeply inclined lamination and possible chevron folding. On the other hand, where images on the pads have a different texture or aspect, or display a loss of continuity between the two sides, they may indicate faulting (Serra 1989). Small depth shifts between similar features on each pad can indicate a microfault. In Fig. 4B2 a small displacement (depth shift) is observed between the two sides of series of microfaults, and the throw can be measured at around 5 cm. The faults make a steep angle (80–90 degrees) with the stratification and appear to show normal displacement.

A continuous change of dips, both in magnitude and azimuth, indicates recumbent folding (Serra 1989), which is commonly present in various slump intervals (Hole 801B). Moreover, a relatively high degree of apparent dips is observed in some intervals (e.g. 42 degrees around depth 252 m, Hole 801B). CSI (silicon yield in decimal fraction) logs (Fig. 9) reveal that the slumping also affects some siliceous sediments (clayey radiolarites/radiolarian claystones) within the volcaniclastic interval, because the log readings correspond to the underlying lithostratigraphic unit which is radiolarian rich (Brown Radiolarites, Figure 2, site 801).

Massive sandstones with fluid escape structures

The sediments of this facies are dominantly medium to fine sand size with a minor proportion of very fine sand to silt size. Individual 'beds' or units (typically 1–8 m thick) are homogeneous with a lack of grading, well to very well sorted and contain many fluid escape structures among which vertical pipes (Fig. 3C) and flame-like pipes are common and locally dominant. Load structures and convolute laminae are rare. The sediments are mainly composed of volcanic glass, igneous rock fragments, pyroxene and (secondary) calcite, with a minor proportion of smectite clays, radiolarians, and red algae.

Unfortunately, wireline logs were not generally obtained for the interval(s) in which this facies occurs. However, in one case we do have a full suite of logs over an interval (292.0–295.0 mbsf, site 800) including massive sandstones with flame-like pipes. This facies is not readily distinguished on the basis of log characteristics from the massive sandstones described below.

Massive structureless sandstones

The sediments of this facies are dominantly fine to medium sand size with some mud size mat-

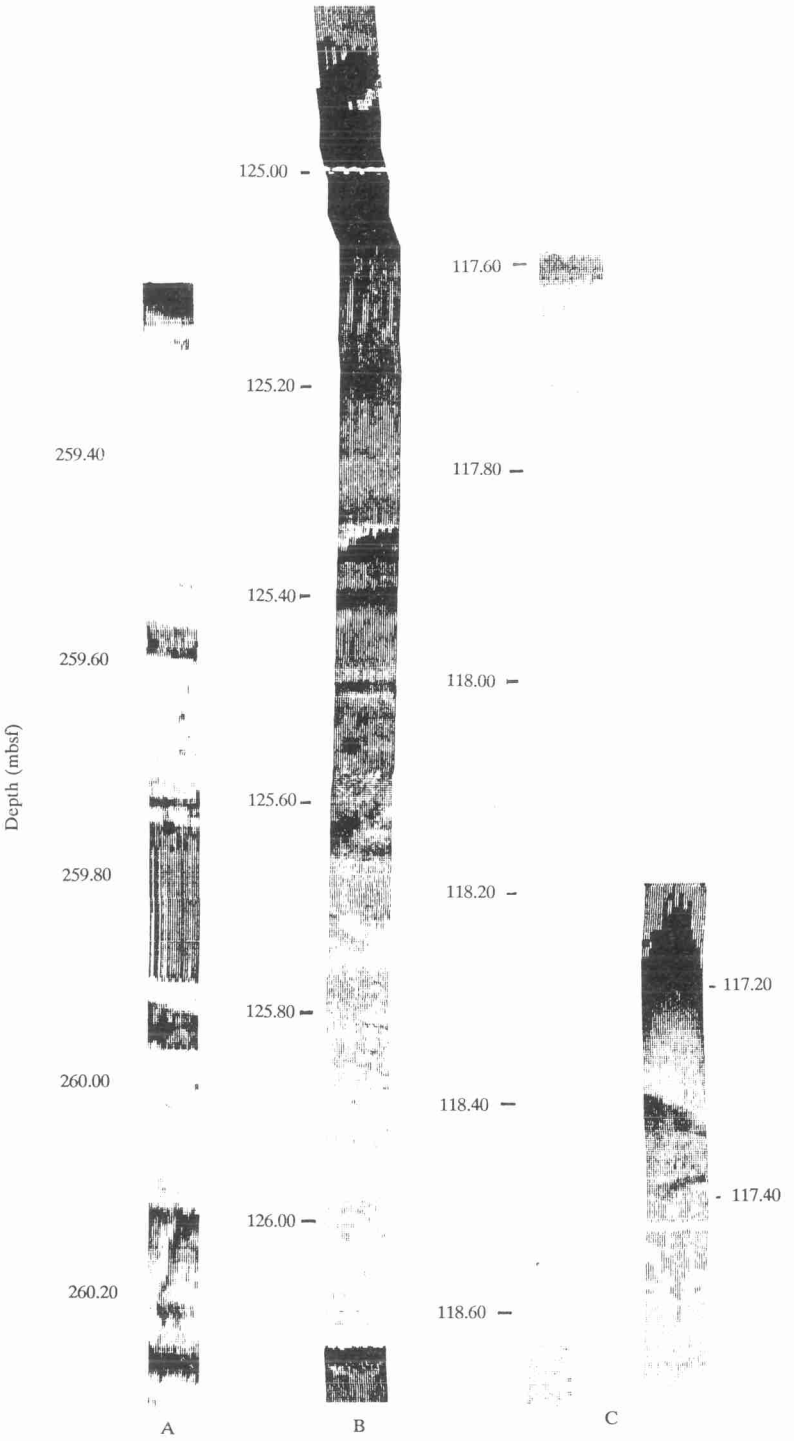

Fig. 7. FMS images of various types of volcaniclastic turbidite beds: A, thin-bedded, medium-grained turbidites; B, thick-bedded, medium-grained turbidites; C, thick-bedded, coarse-grained turbidites.

erial. Individual units or beds (Fig. 3D) appear massive with a general lack of grading, apart from reverse grading in places, and have a typical range of 1–5 m. The sands are moderate to well sorted, and contain rare isolated large clasts (coarse sand to granule size). They are mainly composed of volcanic glass, igneous rock fragments, (secondary) calcite, clays and radiolarians with a minor proportion of calcareous nannofossils, red algae, feldspar and pyroxene.

FMS images reveal a uniform distribution of grey tone within the interval (Fig. 4C) which indicates the structureless nature of the beds and uniform distribution of grain size. Moreover, the presence of the isolated white patches (dots) (more resistive), represents the presence of large clasts as observed in the cores. Where this facies is sufficiently well developed in vertical extent, some of the other logs show similar features. There are consistent dip readings (magnitude and azimuth) in dipmeter logs (Fig. 5) and a very smooth homogeneous aspect of the microresistivity logs (Fig. 5). Gamma ray responses (Fig. 6) are also relatively very smooth and do not show any significant trends in terms of grain size. LIR (lithology indicator ratio) log readings in this facies reveal that the parts adjacent to beds or unit boundaries contain higher silica contents in comparison with the middle portion of the units.

Volcaniclastic turbidites

This facies displays a range of grain sizes from sand to mud grade with granule to pebble size particles at the base of some beds. Individual beds range from 2–400 cm in thickness, show normal grading (Fig. 3E) and contain features typical of coarse-, medium-, and fine-grained turbidites (e.g. Stow 1985, 1986). The sediments are largely composed of volcanic glass, igneous rock fragments, palagonite, pyroxene and (secondary) calcite, with a variable proportion of smectite/chloritic clay, radiolarians, zeolites, feldspar and quartz.

The FMS images clearly document the fining upwards nature of turbidite beds. Graded bedding is indicated by the progressive vertical change in image density, such that an upward increase in grey tone indicates progressive increase in less resistive clay-size particles and hence defines normal graded bedding (Fig. 4D). This is the most common sedimentary structure present within the turbidites, whereas other structures (primary, biogenic and secondary) can be recognized more rarely. These subtle structures are more difficult to resolve through the static normalization image (static pass), although it may be possible to resolve those structures having vertical continuity (resolution) greater than one centimetre using dynamically normalized images. Various types of turbidite beds can be documented on FMS images (Fig. 7).

Dipmeter log readings vary from highly consistent to sequential increase and decrease in magnitude (Fig. 5), which are most probably related to vertical evolution of the turbiditic intervals in terms of grain size and/or sedimentary structure. Moreover, variable dip readings are also observed at the base of some coarse-grained turbidite beds. Microresistivity readings (Fig. 5) support the dip readings in terms of grain size variation. Gamma ray responses (Fig. 6) show a serrated nature reflecting the presence of a series of turbidite beds and, in places, they also indicate fining-upward intervals of turbidite packages.

Calcareous volcaniclastic turbidites

As the name implies, this facies is similar to the volcaniclastic turbidites in terms of sedimentary textures and structures but differs in composition. These turbidites contain 10 to 55% calcareous material, composed of shallow water carbonates (ooids, coralline limestone clasts, red algae), calcareous nannofossils and foraminifers, along with the volcaniclastic and other components that are commonly present in the volcaniclastic turbidite.

FMS, dipmeter, microresistivity, and gamma ray log signatures are similar to those described above for the volcaniclastic turbidite facies. Higher CCA (calcium yield in decimal fraction) log readings (Fig. 8) can be calibrated with the compositional data of turbidite beds and reveal the presence of calcareous turbidite interval(s) in sections with no core recovery.

Pelagites and bioclastic turbidites

Poor core recovery did not allow the clear definition of the sedimentary features within this facies. The sediments are largely composed of clayey radiolarites and radiolarian claystones with a variable proportion of volcaniclastic components.

The FMS images allow us to clearly distinguish pelagic intervals (pelagites, Fig. 4G1) from bioclastic turbidite beds (Fig. 4G2). Erosive lower bedding contacts, normal grading of beds and the fining-upwards nature of turbidite sequences, substantially differ from the horizontally bedded/banded aspect of pelagites (Fig. 3G). Higher CSI (silicon yield in decimal frac-

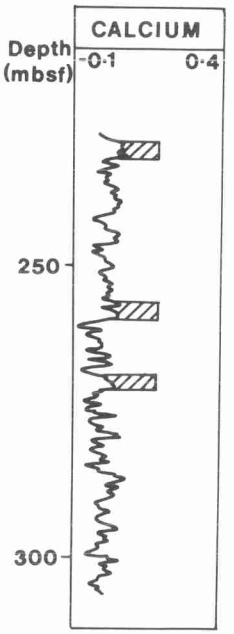

Fig. 8. CCA (calcium yield in decimal fraction) log readings (hatched intervals) revealing the presence of calcareous volcaniclastic turbidites in ODP Hole 800.

tion) log readings (Fig. 9) calibrated with the compositional data and compared with signatures of radiolarian-rich lithostratigraphic unit(s) (Fig. 2, see site 801) reveal the presence of the facies where there is no recovery.

Discussion and conclusions

All the three sites drilled during the ODP Leg 129 have encountered thick volcaniclastic sediments. These sediments show many classical features of the resedimentation processes responsible for their deposition (e.g. Stow 1985, 1986), and their log characteristics, we believe, are applicable to other resedimented successions. Sedimentary features delineated from the recovered cores are initially calibrated with the corresponding FMS images because they have the capability of fine bed resolution. Moreover, the FMS images are the wireline log data which can be compared more closely with the core photographs. If the facies/sedimentary features have sufficient vertical resolution, the other open hole logs including dipmeter–microresistivity and gamma ray readings can be further used to confirm the textural and structural evolution as observed in the FMS images. This study reveals that the combined use of the FMS image (calibrated/non-calibrated), dipmeter–microresistivity and gamma ray logs have made it possible to delineate debrites, slumps, tubidites and massive structureless sandstones as well as to distinguish the one from the other. It also shows that the specific elemental signature(s) of the geochemical combination logs can be used to enhance the compositional aspects of these facies. Higher concentrations of calcium and silica delineated from thin sections are calibrated with the corresponding log readings which are then combined with the image interpretations to distinguish calcareous volcaniclastic turbidites from volcaniclastic turbidites and bioclastic turbidites from pelagites. This combination of wireline logs has been very useful to delineate the vertical extent of facies as well as vertical sequences of facies throughout the volcaniclastic sedimentation and tectonics in the area (Salimullah, in press).

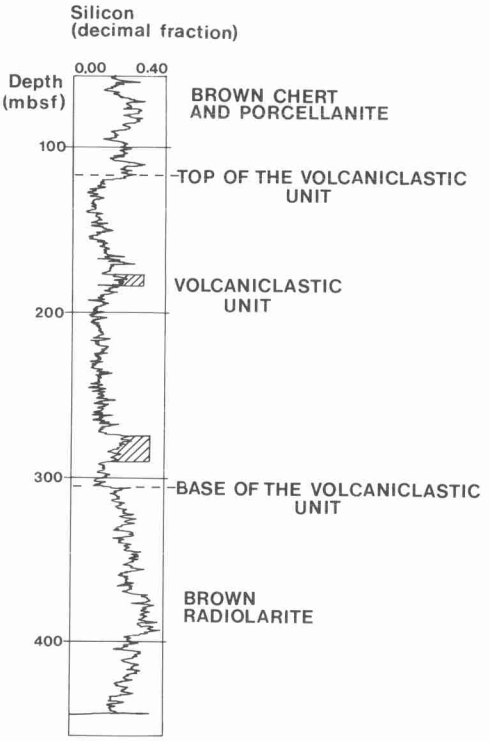

Fig. 9. CSI (silicon yield in decimal fraction) log readings (hatched intervals) revealing the presence of siliceous sediments within the Volcaniclastic Lithologic Unit. These readings largely resemble radiolarian-rich sediments (Brown radiolarites and Brown chert and porcellanites, Fig. 2, site 801) which are underlying and overlying respectively the Volcaniclastic Unit in site 801.

References

EKSTROM, M. P., DAHAN, C., CHEN, M.-Y., LLOYD, P. & ROSSI, D. J. 1987. Formation imaging with microelectrical scanning arrays. *The Log Analyst*, **28**, 306.

HARKER, S. D., MCGANN, G. J., BOURKE, L. T., & ADAMS, J. T. 1990. Methodology of formation micro-scanner image interpretation in Claymore and Scapa Fields (North Sea). *In*: HURST, A., LOVELL, M. A. & MORTON, A. C. (eds) *Geological Applications of Wireline Logs*. Geological Society, London, Special Publication, **48**, 13–23.

KELTS, K. & ARTHER, M. A. 1981. Turbidites after ten years of Deep Sea Drilling—wringing out the mop? *In*: WARME, J. E., DOUGLAS, R. G. & WINTERER, E. L. (eds) *The Deep Sea Drilling Project: A Decade of Progress*. S.E.P.M. Special Publication, **32**, 91–127.

LANCELOT, Y. V., LARSON, R. *et al.* 1990. *Proceedings of the Ocean Drilling Program, Initial Reports*. Ocean Drilling Program, College Station, TX, **129**, 34–39, 91–100, 171–177, 283–321 and 412–435.

LUTHI, S. M. 1990. Sedimentary structures of clastic rocks identified from electrical borehole images. *In*: HURST, A., LOVELL, M. A. & MORTON, A. C. (eds) *Geological Applications of Wireline Logs*. Geological Society, London, Special Publication, **48**, 4–6.

SERRA, O. 1985. *Sedimentary Environments from Wireline Logs*. Schlumberger, 28–35, 160–168.

—— 1986. Information on sedimentary structures. *In: Fundamentals of Well-Log Interpretation, Volume 2*. Elsevier, Amsterdam, 137–152.

—— 1989. *Schlumberger Formation Microscanner Image Interpretation*. Schlumberger Education Services, 16–19, 32–72, 96.

SALIMULLAH, A. R. M. Volcaniclastic facies and sequences, ODP Leg 129 (in press).

STOW, D. A. V. 1984. Cretaceous to recent submarine fans in the southeast Angola Basin. *In*: HAY, W. W., SIBUET, J.-C. *et al. Initial Reports of the D.S.D.P.*, Volume LXXV, 771–784, U.S. Government Printing Office, Washington.

—— 1985. Deep-sea clastics: where we are and where we are going? *In*: BRENCHLEY, P. J. & WILLIAMS, B. P. J. (eds) *Sedimentology: Recent Developments and Applied Aspects*. Geological Society, London, Special Publication, **18**, 67–93.

—— 1986. Deep Clastic Seas. *In*: READING, H. G. (ed.) *Sedimentary Environments and Facies*. Blackwell, Oxford, 399–444.